Electronic Supplementary Information

Band-Structure-Controlled $BiO(ClBr)_{(1-x)/2}I_x$ Solid Solutions for Visible-Light Photocatalysis

Guigao Liu[a,b], Tao Wang[b], Shuxin Ouyang[c], Lequan Liu[c], Haiying Jiang[b], Qing Yu[a,b], Tetsuya Kako[b], and Jinhua Ye*[,a,b,c]

[a] Graduate School of Chemical Science and Engineering, Hokkaido University, Sapporo, Japan.

[b] Environmental Remediation Materials Unit and International Center for Materials Nanoarchitectonics (WPI-MANA), National Institute for Materials Science (NIMS), 1-1 Namiki, Tsukuba, Ibaraki, Japan.

[c] TU-NIMS Joint Research Center, School of Materials Science and Engineering, Tianjin University, 92 Weijin Road, Nankai District, Tianjin, P. R. China.

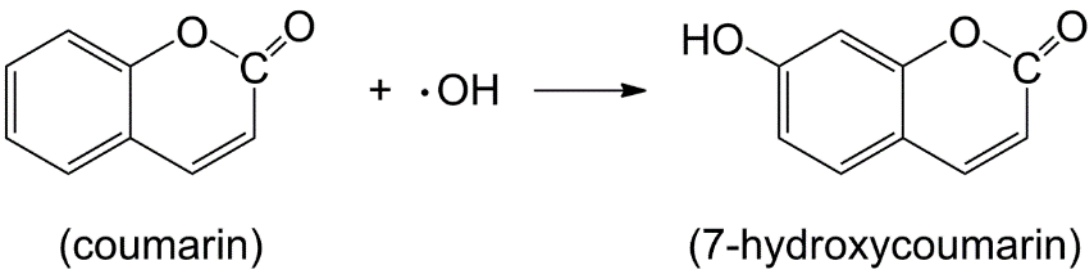

Figure S1. The reaction between •OH and coumarin to form 7-hydroxycoumarin.

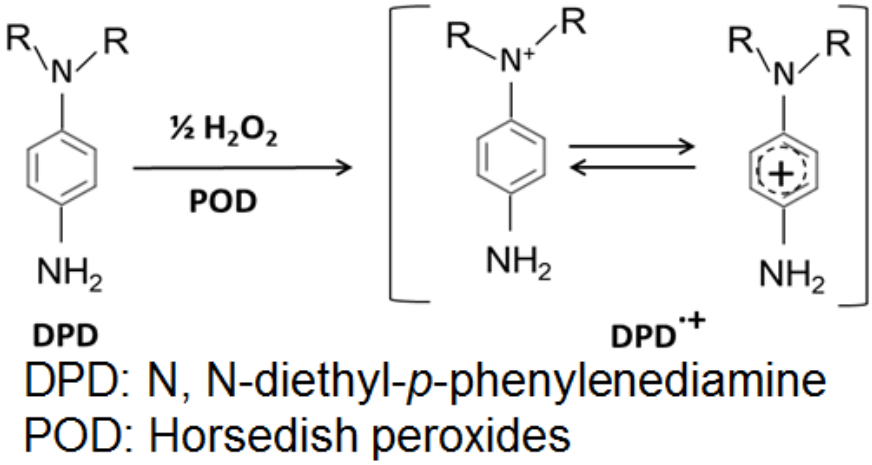

Figure S2. The reaction mechanism of detecting H_2O_2.

The measurement of H_2O_2 was conducted by using the colorimetric DPD method, which is based on the horsedish peroxides (POD)-catalyzed oxidation of N, N-diethyl-*p*-phenylenediamine (DPD) by H_2O_2.[1, 2] Typically, two molecules of DPD could be oxidized by H_2O_2 with POD as catalyst to form the radical cation, $DPD^{\bullet+}$. The reaction is shown in Figure S2.

Since the radical cation, $DPD^{\bullet+}$ can exhibit a stable color with the maximum absorption at 551 nm, the concentration of H_2O_2 in the measured solution can be calculated from the absorbance at 551 nm by considering the following relationship:

$$[H_2O_2]_{sample} = (I^{551} V_{final})/elV_{sample}$$

Where the I^{551} is the absorbance at 551 nm, V_{final} is the final volume after addition of all regents and buffer, V_{sample} is the volume of original sample, e is the constant, l is the path length of optical cell. Since the measurements were conducted under the same conditions, the values of V_{final}, V_{sample}, e and l were kept constant. Thus, the concentration of H_2O_2 can be monitored by the absorption of the solution at 551 nm.

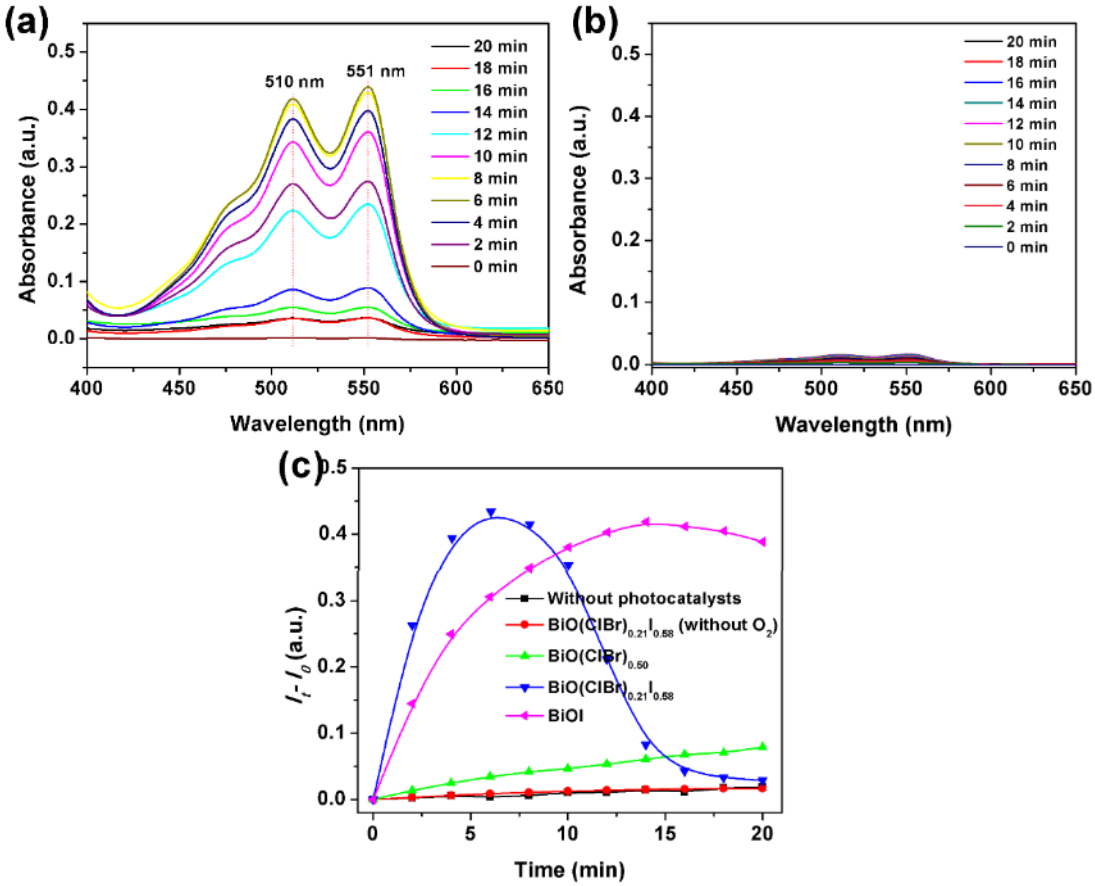

Figure S3. Time-dependent absorption spectra of the DPD/POD-$BiO(ClBr)_{0.21}I_{0.58}$ solution in the presence (a) and absence (b) of O_2. (c) Generation of H_2O_2 during irradiation of different photocatalysts in the presence of methanol as an electron donor (the absorption intensity is an index of H_2O_2 formation).

As shown in Figure S3c, it can be seen that H_2O_2 was not formed in the absence of O_2 though the high active $BiO(ClBr)_{0.21}I_{0.58}$ photocatalysts were added. This result indicates that H_2O_2 was indeed generated from O_2 reduction by excited electrons.[2, 3]

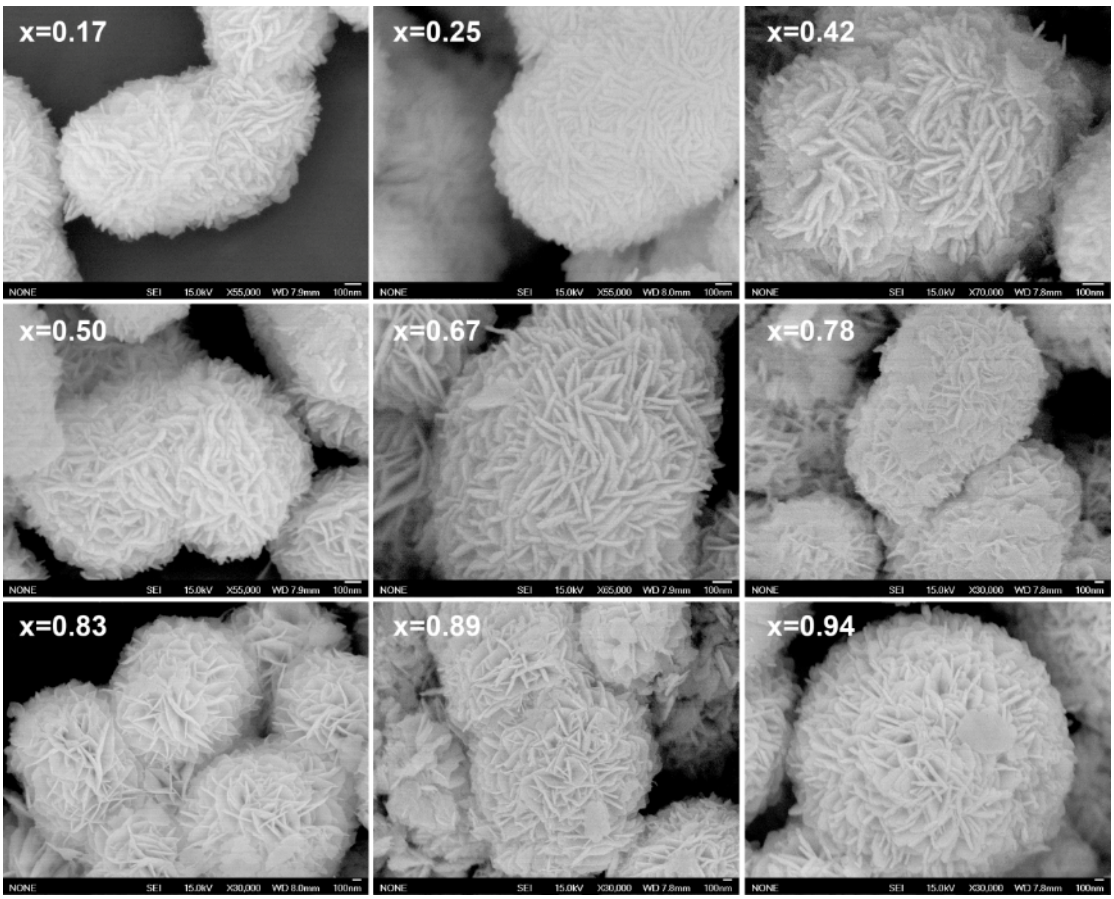

Figure S4. SEM images of $BiO(ClBr)_{(1-x)/2}I_x$ solid solutions.

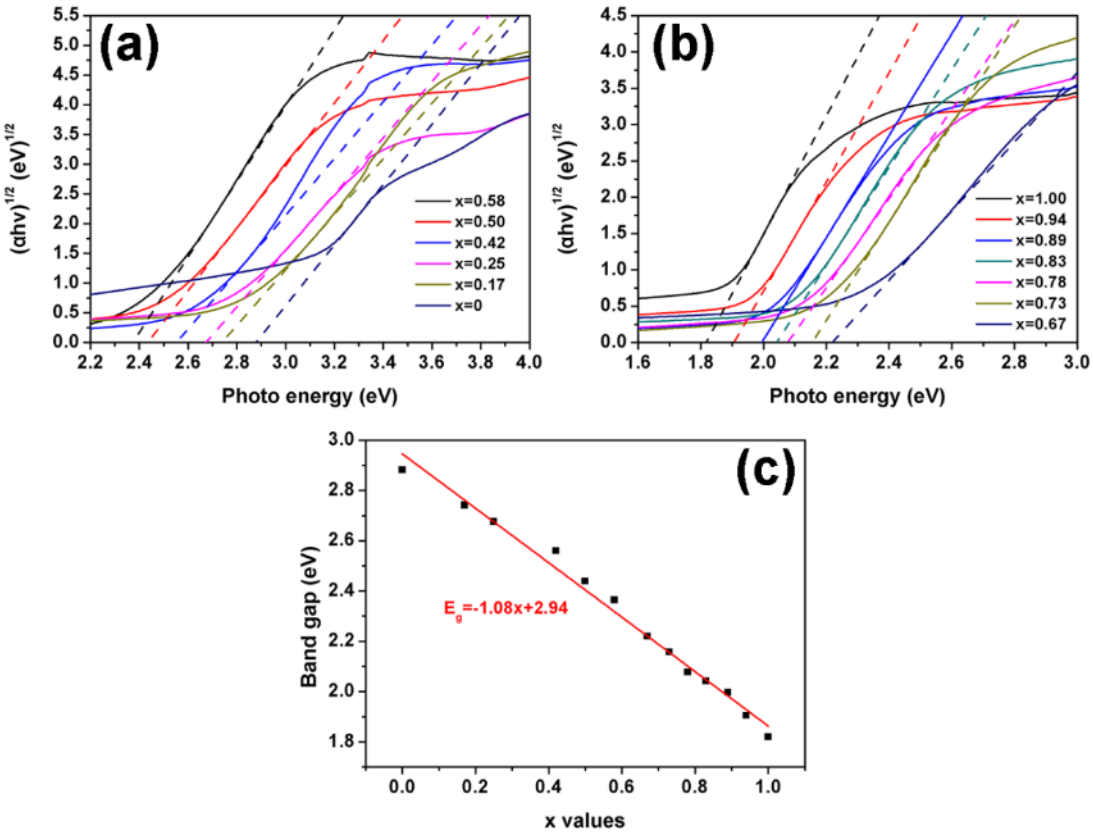

Figure S5. (a and b) $(\alpha h\nu)^{1/2}$ versus hν plots of $BiO(ClBr)_{(1-x)/2}I_x$ solid solutions (c) Band gaps as a function of x in the solid solutions. The fitting line is added to guide the eye.

Table S1. The composition, crystal structures, band gaps and surface areas of $BiO(ClBr)_{(1-x)/2}I_x$ solid solutions.

Materials	Composition ratios for halogen elements (Atomic %)[1]			Lattice parameters (Å)[2]		Band gaps (eV)	Surface areas (m^2/g)
	Cl	Br	I	a	c		
$BiO(ClBr)_{0.5}$	66.2±1.1	33.8±1.1	0	3.895(4)	7.608(6)	2.88	21.7
$BiO(ClBr)_{0.415}I_{0.17}$	62.4±6.1	35.4±6.0	2.2±1.5	3.893(3)	7.717(1)	2.74	41.5
$BiO(ClBr)_{0.375}I_{0.25}$	60.9±6.6	35.3±5.6	3.8±3.0	3.892(7)	7.775(9)	2.68	43.5
$BiO(ClBr)_{0.29}I_{0.42}$	58.8±5.0	36.7±4.7	4.5±2.0	3.898(5)	7.798(3)	2.56	52.4
$BiO(ClBr)_{0.25}I_{0.50}$	52.6±3.8	34.3±3.3	13.1±4.0	3.898(3)	7.839(9)	2.44	61.7
$BiO(ClBr)_{0.21}I_{0.58}$	41.4±4.7	38.6±2.3	20.0±4.3	3.898(5)	7.969(2)	2.36	53.0
$BiO(ClBr)_{0.165}I_{0.67}$	34.6±9.8	33.8±5.0	31.6±5.8	3.910(6)	8.237(5)	2.22	50.9
$BiO(ClBr)_{0.135}I_{0.73}$	29.3±6.4	28.7±1.1	42.0±6.2	3.919(2)	8.867(6)	2.16	52.0
$BiO(ClBr)_{0.11}I_{0.78}$	26.7±3.8	21.0±3.3	52.3±4.2	3.939(3)	8.975(7)	2.08	44.8
$BiO(ClBr)_{0.85}I_{0.83}$	18.3±5.5	17.8±2.2	63.9±4.8	3.946(0)	9.039(5)	2.04	41.0
$BiO(ClBr)_{0.055}I_{0.89}$	11.7±6.9	13.3±4.2	75.0±4.5	3.963(2)	9.087(4)	2.00	32.2
$BiO(ClBr)_{0.03}I_{0.94}$	7.4±1.8	7.7±1.3	84.9±2.9	3.987(6)	9.097(9)	1.91	19.4
BiOI	0	0	100	3.992(4)	9.146(4)	1.82	10.0

[1] The composition ratios for halogen elements were obtained from EDX analysis.
[2] The lattice parameters were calculated from XRD data.

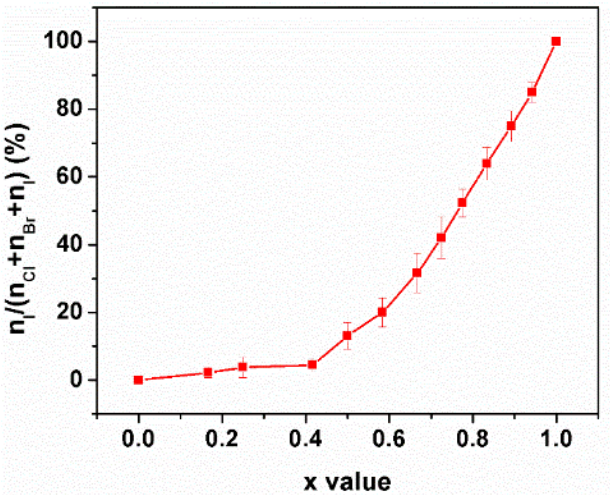

Figure S6. The evolution of composition ratio of I element in $BiO(ClBr)_{(1-x)/2}I_x$ solid solutions.

As shown in Table S1 and Figure S6, when x<0.5, the composition ratio of I element in the solid solutions increases very slowly with x value increasing, which leads to a small change in the lattice parameters (*c* and volume). When 0.5<x<0.78, the composition ratio of I element shows a significant increase from 13.1% to 52.3%. Therefore, in this stage, the lattice parameters are changed greatly. As x is further increased from 0.78 to 1.00, because most of halogen ions in crystals are I^-, the crystal

structure would be relative stable (close to the BiOI crystal structure) and thus the evolution of lattice parameters become slow again (Figure 4a). Additionally, the similar results were also reported by Keller *et al.*.[4] They found that the $BiOCl_{1-x}I_x$ solid solutions were changed from Cl-rich phase to I-rich phase with x increasing and that the lattice parameter *c* showed a sharp increase at the phase transition point.

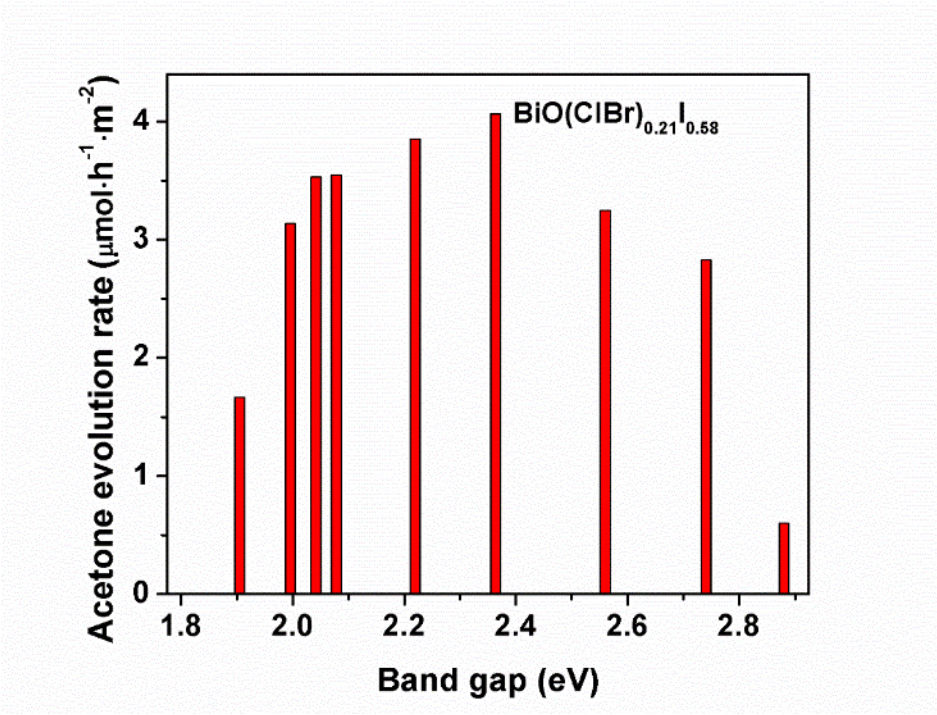

Figure S7. Comparison of surface area normalized acetone evolution rates of $BiO(ClBr)_{(1-x)/2}I_x$ solid solutions with various band gaps.

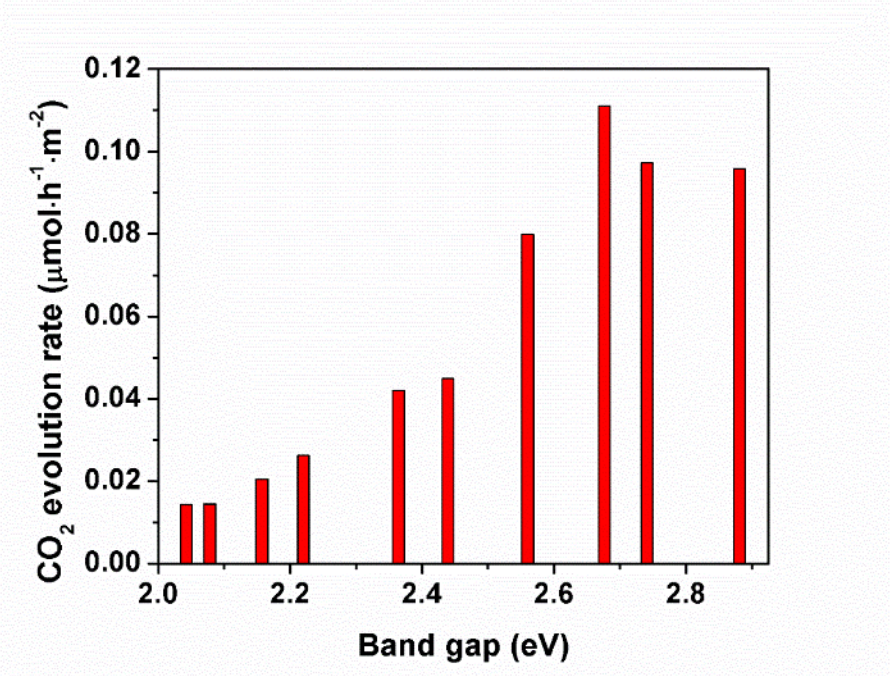

Figure S8. Comparison of surface area normalized CO_2 evolution rates of $BiO(ClBr)_{(1-x)/2}I_x$ solid solutions with various band gaps.

Calculation of the internal quantum efficiency:

The internal quantum efficiency (IQE) was calculated according to the method reported in literature [5] and [6].

Take $BiO(ClBr)_{0.415}I_{0.17}$ for example, under the visible light irradiation, the wavelength of visible light is from 400 to 800 nm, and the light intensity is 30.5 mW/cm^2. The irradiating area is 8.5 cm^2. Therefore, the absorption rate of incident photons (R_p^a) was determined to be 0.05 μmol·sec^{-1} using the following equation: $R_p^a = \int_{400}^{800} S \times \alpha \times I$ (S is the area of the sample, α is the light absorption and I is the light intensity at each wavelength). As for acetone evolution ($CH_3CHOHCH_3+e^-+O_2+H^+ \rightarrow CH_3CHOCH_3+\bullet OH+H_2O$ or $CH_3CHOHCH_3+h^+ \rightarrow CH_3CHOCH_3+e^-+2H^+$), only one photon is required to produce one acetone molecule. In case of CO_2 generation ($CH_3CHOHCH_3+5H_2O+18h^+ \rightarrow 3CO_2+18H^+$), six photons are required to produce one CO_2 molecule. The acetone and CO_2 rates (R_{ACE} and R_{CO2}) were

determined to be 12.8 and 0.44 μmol·h^{-1} (Figure 6a). Thus, the IQE of $BiO(ClBr)_{0.415}I_{0.17}$ could be calculated using the following equation:

$IQE = (R_{ACE} + 6\times R_{CO2}) / R_p^a \times 100\%$

$= ((12.8+ 6 \times 0.44)/3600)$ μmol·sec^{-1} / 0.05 μmol·sec^{-1} × 100%

= 8.6%

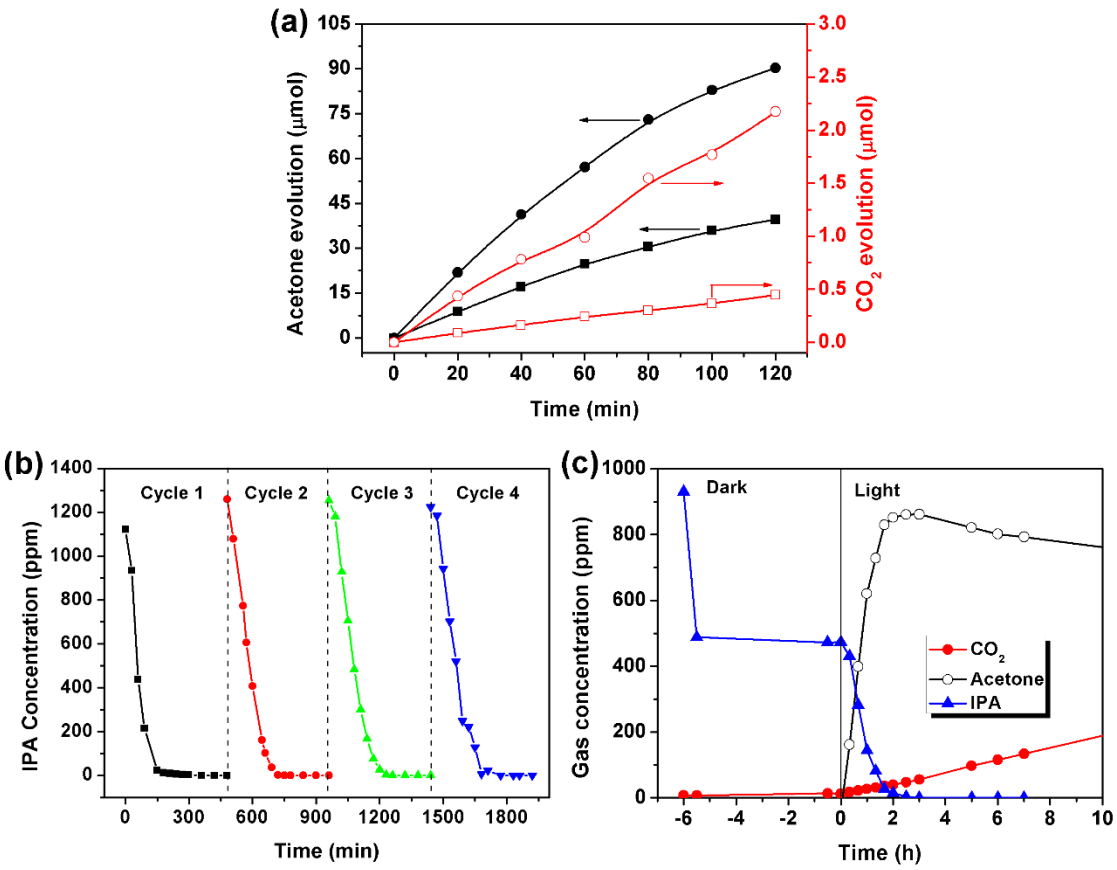

Figure S9. (a) Curves of acetone (filled symbols) and CO_2 evolution (open symbols) in photodegradation of IPA over $BiO(ClBr)_{0.21}I_{0.58}$ (■ □) and $BiO(ClBr)_{0.21}I_{0.58}$-1.0 wt% Pt (● ○). The loading Pt was conducted by a typical photodepostion method using methanol as scavenger for holes. (b) Cycling degradation of IPA over $BiO(ClBr)_{0.21}I_{0.58}$ photocatalysts. (c) The concentration evolutions of IPA, acetone and CO_2 during the first ten hours of long-term photodegradation experiment over $BiO(ClBr)_{0.21}I_{0.58}$ photocatalysts.

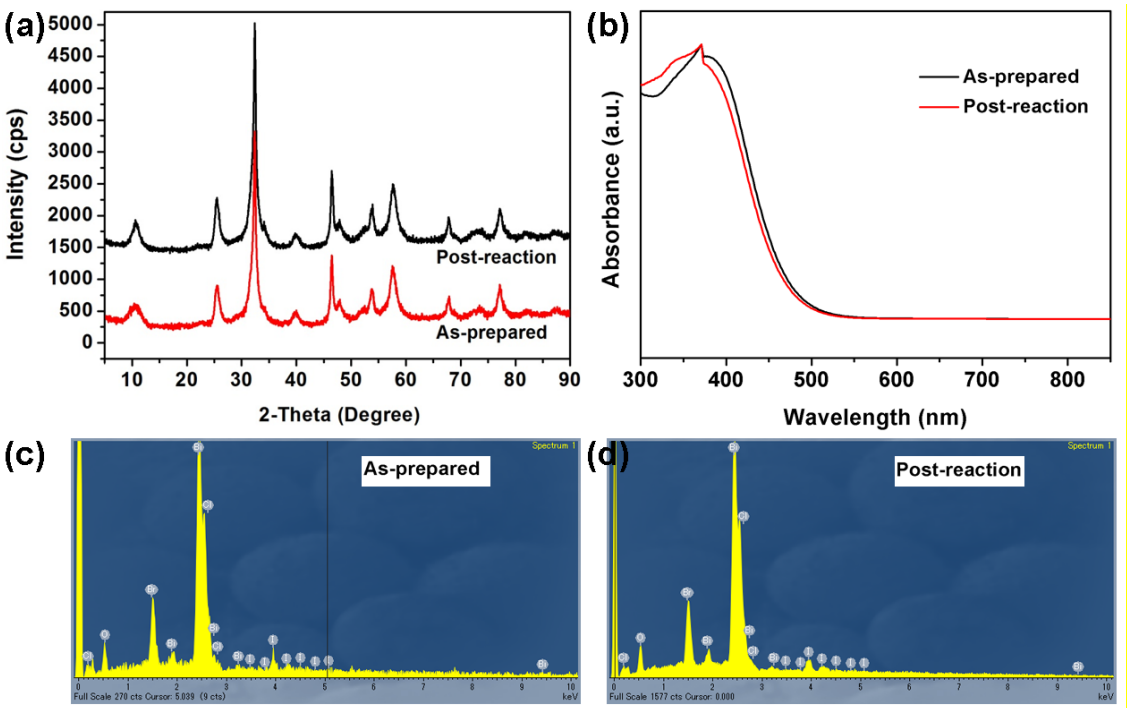

Figure S10. (a) XRD patterns, (b) UV-vis absorption spectra and (c and d) EDS spectra of as-prepared and post-reaction $BiO(ClBr)_{0.21}I_{0.58}$ photocatalysts.

Table S2. The composition ratios of halogen elements and the lattice parameters of as-prepared and post-reaction $BiO(ClBr)_{0.21}I_{0.58}$ photocatalysts.

$BiO(ClBr)_{0.21}I_{0.58}$	**Composition ratios for halogen elements (Atomic %)[1]**			**Lattice parameters (Å)[2]**	
	Cl	Br	I	*a*	*c*
As-prepared	41.4±4.7	38.6±2.3	20.0±4.3	3.898(5)	7.969(2)
Post-reaction	40.8±3.8	38.9±2.5	20.3±1.3	3.895(0)	7.960(3)

[1] The composition ratios for halogen elements were obtained from EDX analysis.
[2] The lattice parameters were calculated from XRD data.

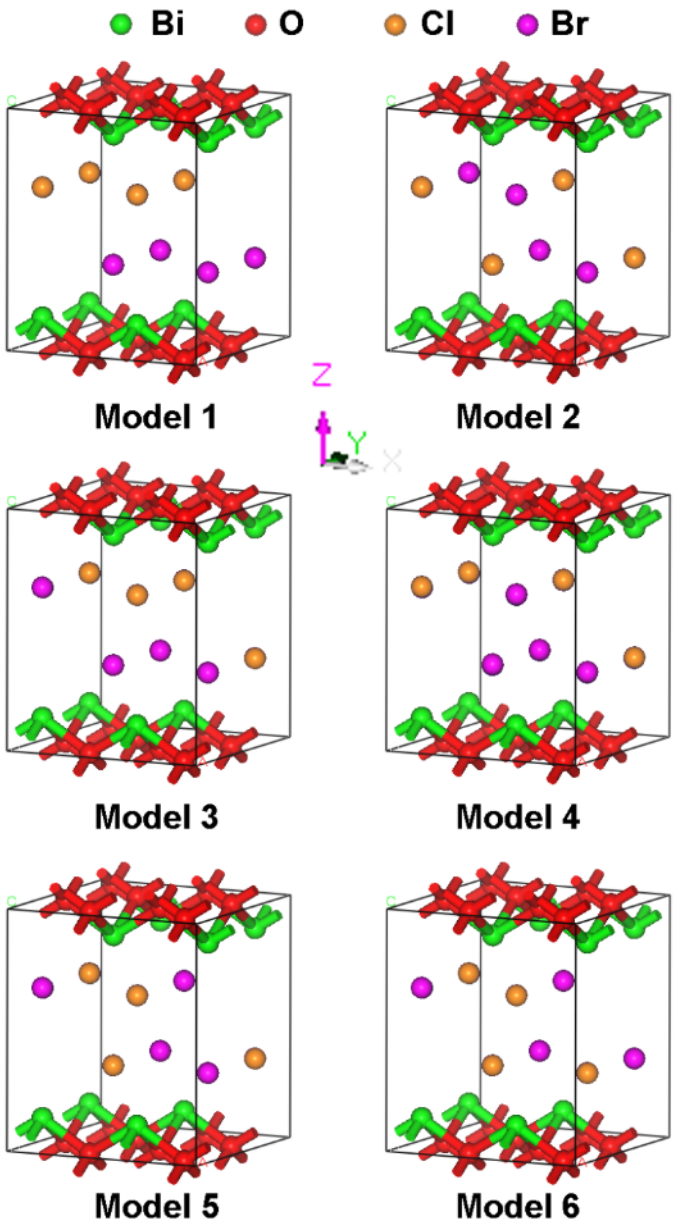

Figure S11. Six possible models of $BiO(ClBr)_{0.5}$ for geometry optimization.

The band structures of these six models were calculated and similar results were obtained. Since the total energy of Model 1 is the lowest (Table S2), indicating this structure is the most stable, its band structure was chosen as a representative for discussion in Figure 8.

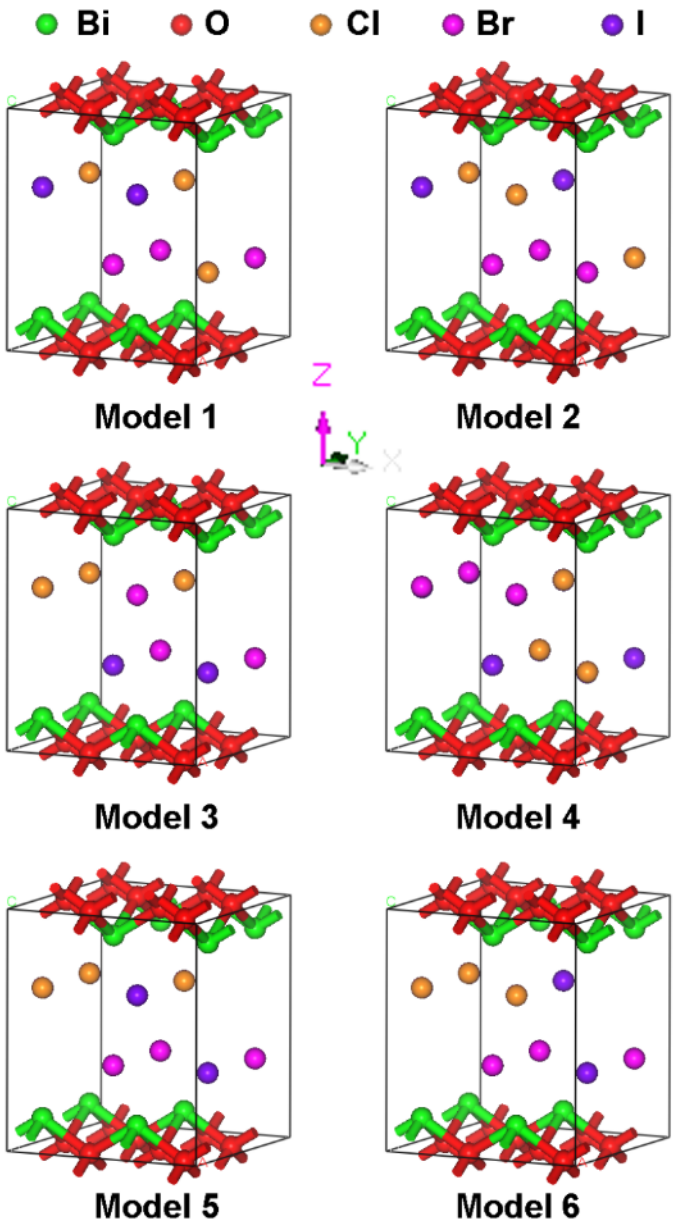

Figure S12. Six possible models of $BiO(ClBr)_{0.375}I_{0.25}$ for geometry optimization. The band structures of these six models were calculated and similar results were obtained. Since the total energy of Model 2 is the lowest (Table S2), indicating this structure is the most stable, its band structure was chosen as a representative for discussion in Figure 8.

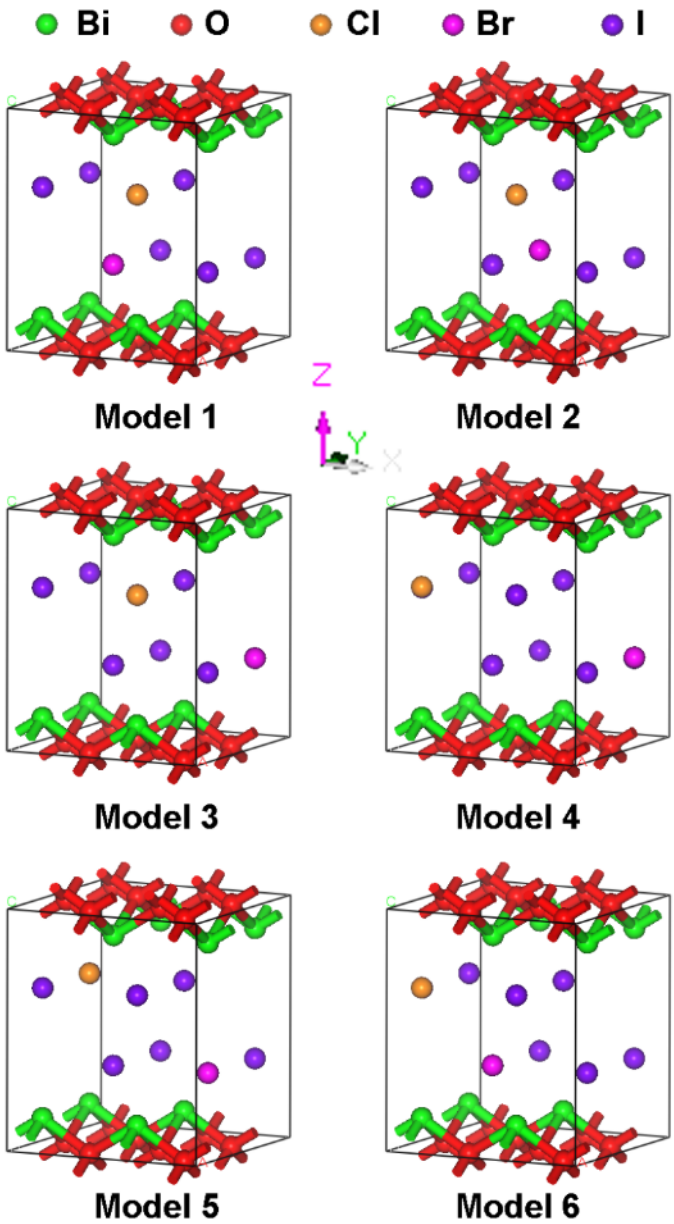

Figure S13. Six possible models of $BiO(ClBr)_{0.125}I_{0.75}$ for geometry optimization. The band structures of these six models were calculated and similar results were obtained. Since the total energy of Model 6 is the lowest (Table S2), indicating this structure is the most stable, its band structure was chosen as a representative for discussion in Figure 8.

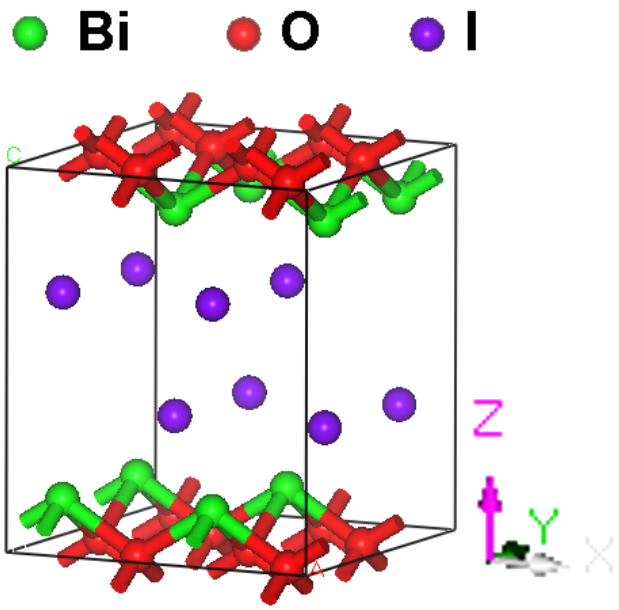

Figure S14. The model of BiOI for geometry optimization.

Table S3. Total energies, lattice parameters and band gaps of $BiO(ClBr)_{0.5}$, $BiO(ClBr)_{0.375}I_{0.25}$, $BiO(ClBr)_{0.125}I_{0.75}$ and BiOI.[1]

Samples	model	Total energy (eV)	Supercell lattice parameters (Å)			Volume of supercell (Å^3)	Unit cell lattice parameters (Å)			Volume of unit cell (Å)	Band gap (eV)
			A	*B*	*C*		*a*	*b*	*c*		
$BiO(ClBr)_{0.5}$	Model 1	-7839.47537	7.56651	7.56404	7.58454	434.089	3.78325	3.78202	7.58454	108.522	2.00
	Model 2	-7839.42109	7.56500	7.56501	7.62277	436.245	3.78250	3.78251	7.62277	109.061	1.92
	Model 3	-7839.44403	7.56622	7.56600	7.59908	435.017	3.78311	3.78300	7.59908	108.754	1.95
	Model 4	-7839.43855	7.56546	7.56590	7.63057	436.769	3.78273	3.78295	7.63057	109.192	1.96
	Model 5	-7839.41820	7.56568	7.56568	7.62936	436.700	3.78284	3.78284	7.62936	109.175	1.92
	Model 6	-7839.42621	7.56453	7.56543	7.63214	436.779	3.78227	3.78272	7.63214	109.195	1.93
$BiO(ClBr)_{0.375}I_{0.25}$	Model 1	-7692.79850	7.61257	7.57579	8.48865	489.528	3.80629	3.78790	8.48865	122.382	1.58
	Model 2	-7692.85220	7.57773	7.57937	8.57991	492.782	3.78887	3.78969	8.57991	123.196	1.90
	Model 3	-7692.82865	7.60840	7.58978	8.31624	480.270	3.80420	3.79489	8.31624	120.068	1.55
	Model 4	-7692.83143	7.58908	7.59211	8.45786	487.317	3.79454	3.79606	8.45786	121.829	1.85
	Model 5	-7692.74677	7.58441	7.58167	8.68032	499.015	3.79221	3.79084	8.68032	124.754	1.96
	Model 6	-7692.78195	7.58868	7.58376	8.54354	491.615	3.79434	3.79188	8.54354	122.904	1.81
$BiO(ClBr)_{0.125}I_{0.75}$	Model 1	-7400.09271	7.69321	7.69032	9.10761	538.843	3.84661	3.84516	9.10761	134.711	1.51
	Model 2	-7400.09295	7.69252	7.69246	9.10386	538.713	3.84626	3.84623	9.10386	134.678	1.51
	Model 3	-7400.09146	7.69276	7.69235	9.11164	539.183	3.84638	3.84618	9.11164	134.796	1.51
	Model 4	-7400.08069	7.69609	7.69028	9.10346	538.787	3.84805	3.84514	9.10346	134.697	1.50
	Model 5	-7400.09228	7.69283	7.69309	9.10542	538.871	3.84642	3.84655	9.10542	134.718	1.51
	Model 6	-7400.09339	7.68753	7.69486	9.10783	538.767	3.84377	3.84743	9.10783	134.692	1.52
BiOI	Model 1	-7253.84451	7.75167	7.75170	9.00978	541.385	3.87584	3.87585	9.00978	135.346	1.41

[1] The data were calculated by density functional theory (DFT).

Table S4. The averages of lattice parameters and band gaps of $BiO(ClBr)_{0.5}$, $BiO(ClBr)_{0.375}I_{0.25}$, $BiO(ClBr)_{0.125}I_{0.75}$ and BiOI.[1]

Samples	Average of unit cell lattice parameters (Å)			Average of volume of unit cell (Å)	Average of band gap (eV)
	a	*b*	*c*		
$BiO(ClBr)_{0.5}$	3.78278±0.00037	3.78267±0.00037	7.61641±0.01986	108.983±0.282	1.95±0.03
$BiO(ClBr)_{0.375}I_{0.25}$	3.79674±0.00693	3.79188±0.00311	8.51109±0.12307	122.522±1.556	1.78±0.17
$BiO(ClBr)_{0.125}I_{0.75}$	3.84625±0.00138	3.84611±0.00087	9.10664±0.00306	134.715±0.042	1.51±0.01
BiOI	3.87584	3.87585	9.00978	135.346	1.41

[1] The averages were calculated using the date in Table S2.

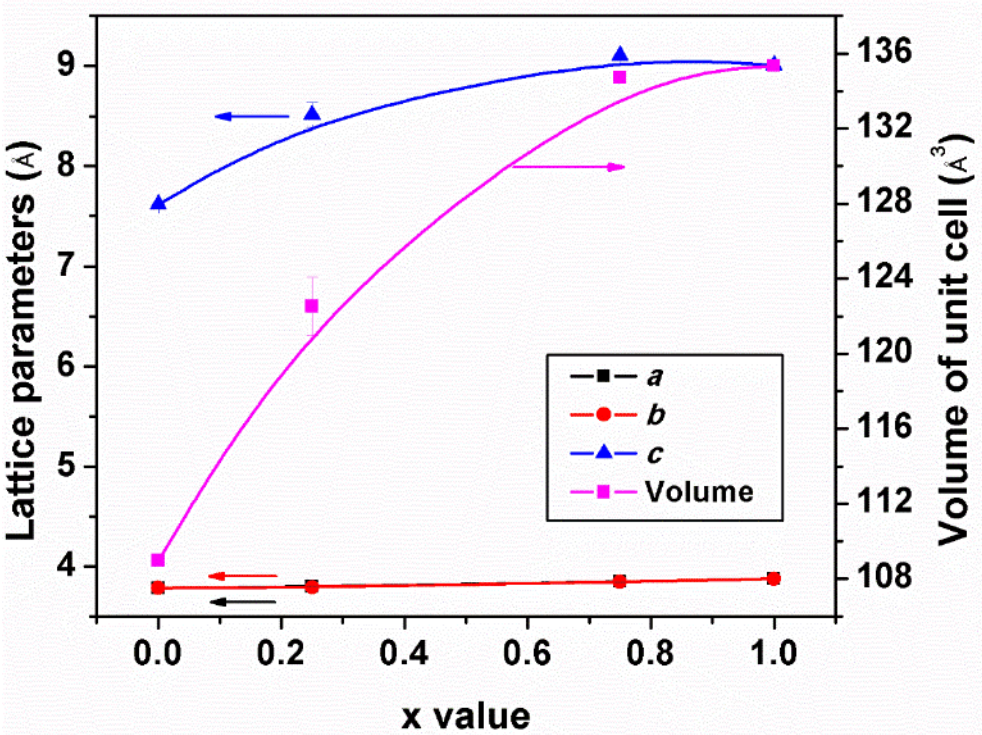

Figure S15. Lattice parameters of $BiO(ClBr)_{(1-x)/2}I_x$ solid solutions obtained from DFT calculation.

As shown in Figure S15, it is found that the c parameter is more modified than the a parameter by the halogen substitution, well consistent with the experimental results (Figure 4a)

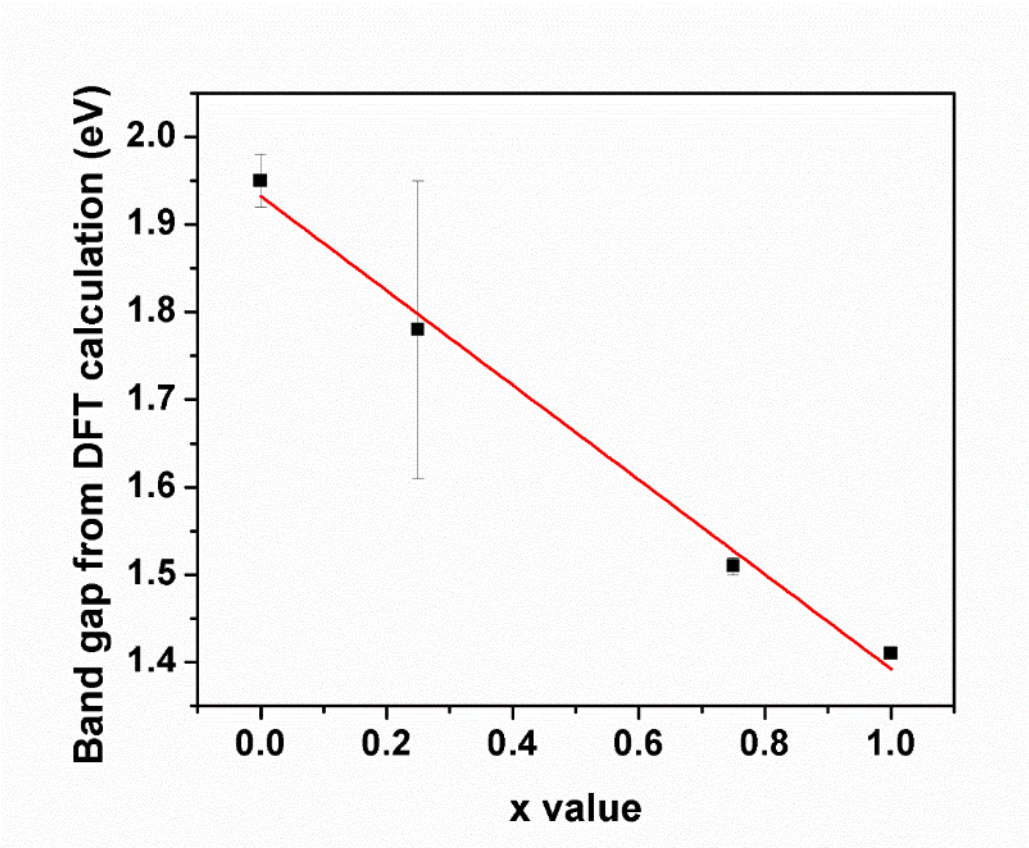

Figure S16. Band gaps of $BiO(ClBr)_{(1-x)/2}I_x$ solid solutions obtained from DFT calculation.

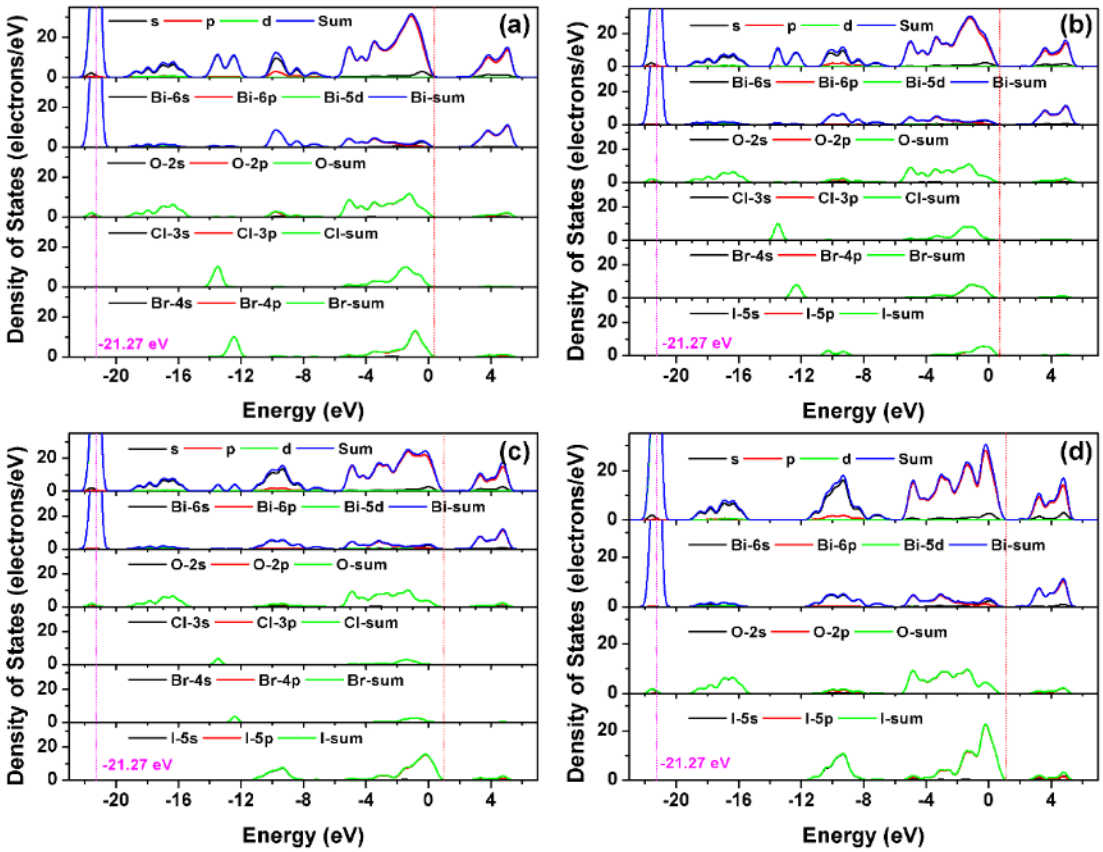

Figure S17.The density of states (DOS) and partial density of states (PDOS) for (a) $BiO(ClBr)_{0.5}$, (b) $BiO(ClBr)_{0.375}I_{0.25}$, (c) $BiO(ClBr)_{0.125}I_{0.75}$ and (d) BiOI, respectively. In order to investigate the evolution of valence band more clearly, the Bi (5d) levels were chosen as the representative core levels as they are the deepest in levels in all the materials.[7, 8]

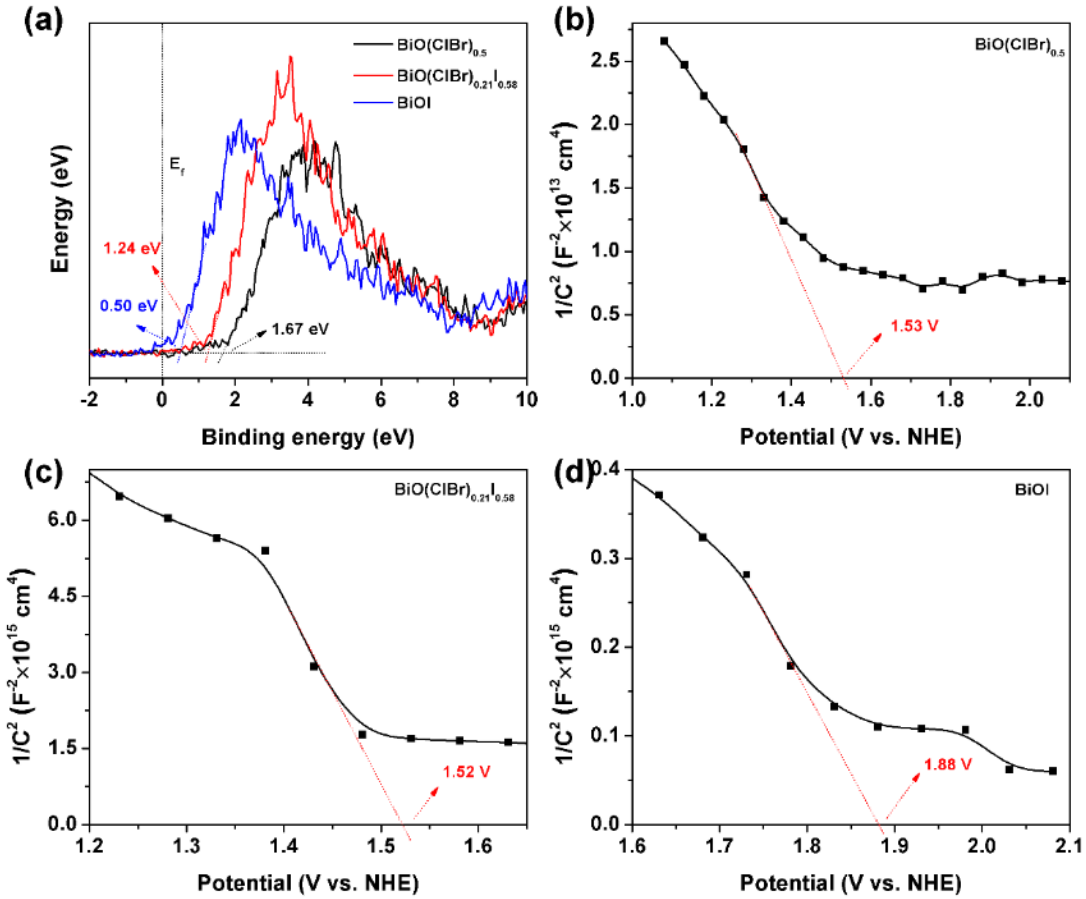

Figure S18. The valence band XPS spectra (a) and Mott–Schottky plots (b-d) of the $BiO(ClBr)_{0.5}$, $BiO(ClBr)_{0.21}I_{0.58}$, and BiOI. The Mott–Schottky curves were measured at 1000 Hz in 0.5 M Na_2SO_4 solution. As calculated from the x intercepts of the linear portion of the Mott–Schottky data, the flat-band potentials are estimated to be 1.53, 1.52 and 1.88 V versus a normal hydrogen electrode (NHE) for $BiO(ClBr)_{0.5}$, $BiO(ClBr)_{0.21}I_{0.58}$ and BiOI, respectively.

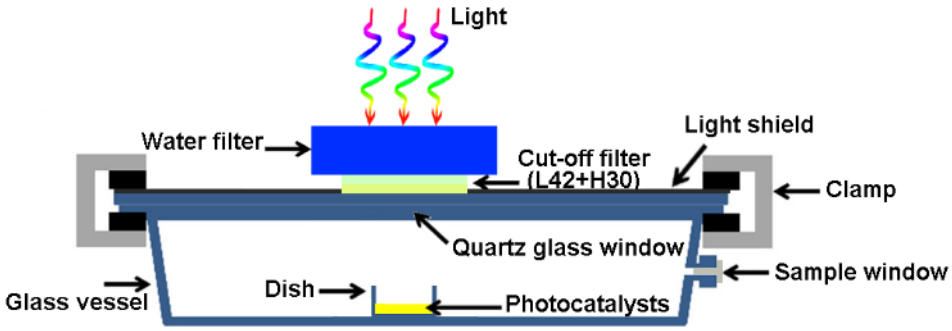

Figure S19. The sketch of the experimental set up for the photodecomposition of IPA in the gas phase.

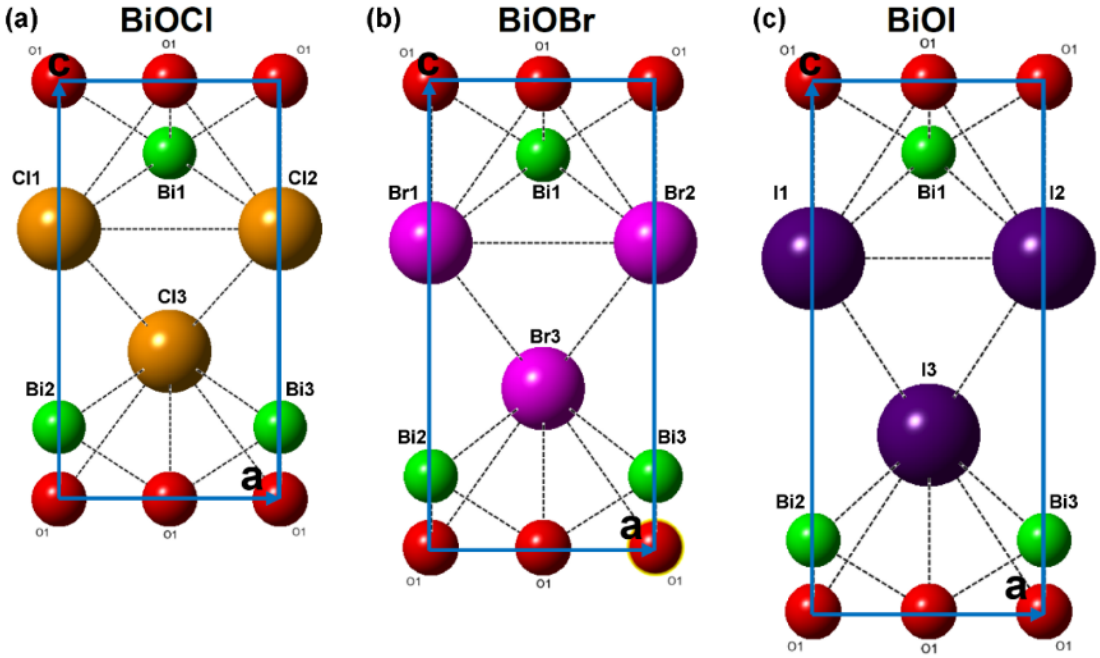

Figure S20. The crystal structure of (a) BiOCl, (b) BiOBr, and (c) BiOI as seen from [010].

Table S5. Ionic radius and bond lengths in BiOCl, BiOBr, and BiOI[4, 9]

Ions	Ionic radius (Å)	BiOCl		BiOBr		BiOI	
Bi^{3+}	1.03	Bonds and bond lengths (Å)		Bonds and bond lengths (Å)		Bonds and bond lengths (Å)	
O^{2-}	1.40	Bi1-Cl1,Cl2	3.059	Bi1-Br1,Br2	3.170	Bi1-I1,I2	3.362
Cl^{-}	1.81	Bi2,Bi3-Cl3	3.059	Bi2,Bi3-Br3	3.170	Bi2,Bi3-I3	3.362
Br^{-}	1.96	Cl1-Cl2	3.887	Br1-Br2	3.923	Cl1-Cl2	3.995
I^{-}	2.20	Cl1,Cl2-Cl3	3.487	Br1,Br2-Br3	3.763	I1,I2-Cl3	4.162

Table S6. (001) peak position, full width at half maximum (FWHM) and calculated crystallite size of $BiO(ClBr)_{(1-x)/2}I_x$ solid solutions.

x value	(001) Peak position (°2Theta)	FWHM (°2Theta)	Calculated crystallite size by Scherrer formula (nm)
0	11.49	0.83	9.49
0.17	11.36	1.21	6.51
0.25	11.32	1.23	6.40
0.42	11.09	1.50	5.25
0.50	10.68	2.22	3.56
0.58	10.91	1.91	4.13
0.67	10.41	1.77	4.46
0.73	9.64	1.73	4.57
0.78	9.62	1.23	6.40
0.83	9.52	1.40	5.62
0.89	9.64	1.40	5.62
0.94	9.65	0.60	13.05
1.00	9.63	0.27	29.36

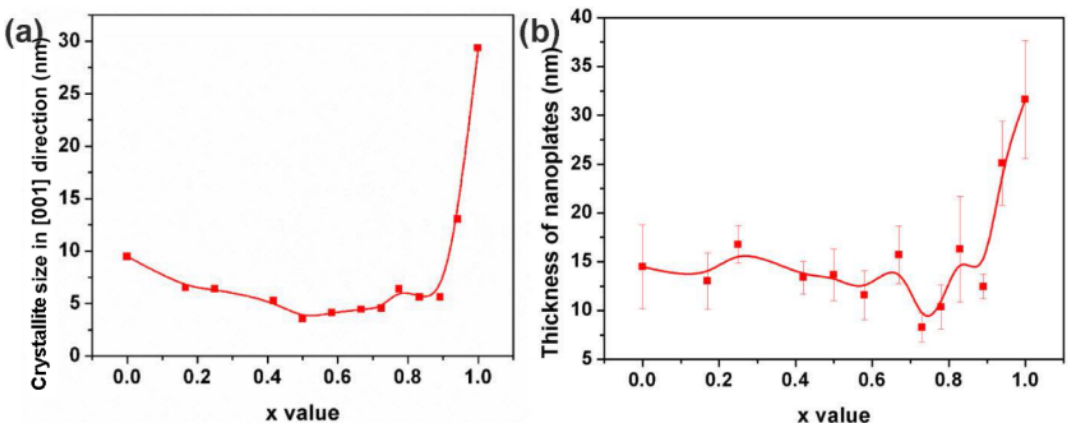

Figure S21. (a) The crystallite size calculated from the (001) peak in XRD pattern and (b) the thickness of nanoplates measured from SEM images.

As shown in Figure S21a and Table S6, the crystallite size in 001 direction was decreased gradually with x increased from 0 to 0.50. However, when x was further increased to 1.00, a significant increase in crystallite size was observed. These results are consistent with SEM images of $BiO(ClBr)_{(1-x)/2}I_x$ solid solutions, which showed that the thickness of the nanoplates was decreased firstly and increased afterward with the

increase of x value (Figure 1, Figure S4 and Figure S21b).

References

1. A. P. Davis and C. P. Huang, *Water Res.*, 1990, **24**, 543-550.
2. J. Guo, S. Ouyang, H. Zhou, T. Kako and J. Ye, *J. Phys. Chem. C*, 2013, **117**, 17716-17724.
3. H.-Y. Jiang, G. Liu, M. Li, J. Liu, W. Sun, J. Ye and J. Lin, *Appl. Catal., B*, 2015, **163**, 267-276.
4. E. Keller and V. Kramer, *Z. Naturforsch. B*, 2005, **60**, 1255.
5. S. N. Habisreutinger, L. Schmidt-Mende and J. K. Stolarczyk, *Angew. Chem. Int. Ed.*, 2013, **52**, 7372-7408.
6. M. Liu, X. Qiu, M. Miyauchi and K. Hashimoto, *J. Am. Chem. Soc.*, 2013, **135**, 10064-10072.
7. D. J. Temple, A. B. Kehoe, J. P. Allen, G. W. Watson and D. O. Scanlon, *J. Phys. Chem. C*, 2012, **116**, 7334-7340.
8. W. L. Huang and Q. Zhu, *Comput. Mater. Sci.*, 2008, **43**, 1101-1108.
9. R. Shannon, *Acta. Cryst. A*, 1976, **32**, 751-767.